Assessing the Effects of Data Selection with the DAO Physical-Space Statistical Analysis System*

STEPHEN E. COHN, ARLINDO DA SILVA, JING GUO,+ META SIENKIEWICZ,+ AND DAVID LAMICH+

Data Assimilation Office, NASA/Goddard Space Flight Center, Greenbelt, Maryland

(Manuscript received 3 April 1997, in final form 22 December 1997)

ABSTRACT

Conventional optimal interpolation (OI) analysis systems solve the standard statistical analysis equations approximately, by invoking a local approximation and a data selection procedure. Although solution of the analysis equations is essentially exact in the recent generation of global spectral variational analysis systems, these new systems also include substantial changes in error covariance modeling, making it difficult to discern whether improvements in analysis and forecast quality are due to exact, global solution of the analysis equations, or to changes in error covariance modeling.

The formulation and implementation of a new type of global analysis system at the Data Assimilation Office, termed the Physical-space Statistical Analysis System (PSAS), is described in this article. Since this system operates directly in physical space, it is capable of employing error covariance models identical to those of the predecessor OI system, as well as more advanced models. To focus strictly on the effect of global versus local solution of the analysis equations, a comparison between PSAS and OI analyses is carried out with both systems using identical error covariance models and identical data. Spectral decomposition of the analysis increments reveals that, relative to the PSAS increments, the OI increments have too little power at large horizontal scales and excessive power at small horizontal scales. The OI increments also display an unrealistically large ratio of divergence to vorticity. Dynamical imbalances in the OI-analyzed state can therefore be attributed in part to the approximate local method of solution, and are not entirely due to the simple geostrophic constraint built into the forecast error covariance model. Root-mean-square observation minus 6-h forecast errors in the zonal wind component are substantially smaller for the PSAS system than for the OI system.

1. Introduction

Practical implementation of statistical analysis schemes requires many simplifying assumptions and approximations for computational feasibility. In conventional optimal interpolation (OI) schemes the analysis problem is *localized*: a local approximation is employed to solve the analysis equations either grid point by grid point (e.g., Bergman 1979) or in small volumes (Lorenc 1981), and a data selection procedure is invoked to reduce the quantity of observations available locally to a sufficiently small number capable of being handled by the computational resources. The purpose of this article is to examine the limitations of this localization of the analysis problem in an operational data assimilation system.

The term optimal interpolation is generally used to refer to a statistical analysis scheme that takes the following as basic simplifications: (a) isotropy: horizontal error correlation functions are isotropic; (b) separability: three-dimensional error correlation functions are the product of vertical and horizontal correlation functions; (c) geostrophy: analyses are multivariate in the wind and mass variables, with a geostrophic-like balance constraint built into the wind/mass error covariance model; (d) local approximation: the analysis at each grid point or in each volume incorporates observational data only in some neighborhood of that grid point or volume; (e) data selection: only some portion of the observations in that neighborhood is actually included in the analysis. As of this writing, many numerical weather prediction centers have replaced (or will soon replace) OI schemes with global variational analysis systems that relax or remove the local approximation and avoid data selection altogether (Parrish and Derber 1992; Courtier et al. 1998; Rabier et al. 1998; Andersson et al. 1998). Since these new analysis schemes are formulated directly in spectral (spherical harmonic) space, rather than in physical space like OI schemes, they also include changes

* Dedicated to the memory of Dr. James W. Pfaendtner, who established much of the computational foundation for the Physical-space Statistical Analysis System.

+ Additional affiliation: General Sciences Corporation, Laurel, Maryland, a subsidiary of Science Applications International Corporation.

Corresponding author address: Dr. Stephen E. Cohn, Data Assimilation Office, Code 910.3, NASA/GSFC, Greenbelt, MD 20771.
E-mail: cohn@dao.gsfc.nasa.gov

in error covariance modeling and imposed wind/mass balance constraints. In the process of replacing OI schemes by global analysis schemes, therefore, establishing the impact of each individual change on overall data assimilation system performance is not always immediate.

The Physical-space Statistical Analysis System (PSAS) being developed at the Data Assimilation Office (DAO) of NASA's Goddard Space Flight Center is a new type of global analysis system designed to replace the OI analysis component of the Goddard Earth Observing System Data Assimilation System (GEOS DAS; Pfaendtner et al. 1995). It differs substantially from current global variational analysis systems in that it is formulated directly in physical space, rather than in a spectral space. This new system is designed specifically to accomodate a number of incremental improvements over the OI component of the GEOS DAS. In particular, the initial implementation described in this article employs error covariance statistics identical to those of the OI system, including the simple geostrophic balance constraint relating height and wind error statistics. This first implementation of PSAS differs from the OI system only in the numerical method used to solve for the analysis increments: a global conjugate gradient solver includes all available observations to produce the analyzed fields. While improved error covariance models are being developed, we can isolate and study the impact of a global analysis scheme on the performance of the GEOS DAS.

This article is organized as follows. The design goals of PSAS and its numerical algorithm are described in section 2. This section also details the relationship between PSAS and OI schemes, and between PSAS and global spectral variational analysis schemes. In section 3, we outline the components of version 1 of the GEOS DAS (GEOS-1 DAS), the original OI-based data assimilation system developed at the DAO. Section 4 describes the design of our experiments and presents the results of comparisons between PSAS analyses and those of the GEOS-1 DAS. Concluding remarks appear in section 5.

2. The Physical-space Statistical Analysis System

a. Design objectives

At the time the DAO was formed, in February 1992, plans were initiated to develop a new statistical analysis system called the Physical-space Statistical Analysis System. PSAS was designed to meet the following five requirements.

1) To establish and remove the effects of data selection in the GEOS-1 OI system. This objective requires PSAS to be capable of using forecast and observation error covariance models identical to those specified in the OI system, but to solve the analysis equations globally rather than locally.
2) To obtain proper sensitivity to all data and to all error covariance specifications. In the OI implementation of Baker et al. (1987), for instance, introducing geographically dependent forecast error covariances had little impact on OI analyses. It is likely that global solution of the analysis equations demanded by objective 1 would reveal much more responsiveness, forcing one to pay careful attention to error covariance formulations, in particular to global wind/mass balance constraints. Recent experiments with the PSAS system (not described here) have in fact demonstrated strong sensitivity to these formulations and will be described in future publications.
3) To permit assimilation of new data types that are not state variables. A great wealth of data, mostly from spaceborne remote-sensing devices, will become available in coming years. Data selection would become an increasingly onerous and ad hoc procedure for these data. More importantly, many of these data, especially if assimilated in raw form (e.g., radiances or backscatter) rather than as retrieved products, are neither state variables nor linearly related to state variables. While some types of data that are not state variables, such as total precipitable water, have been successfully assimilated with the OI methodology (Ledvina and Pfaendtner 1995), global formulation of the analysis problem, in which observation operators are defined explicitly, provides a natural framework for assimilating these data types (e.g., Eyre et al. 1993; Derber and Wu 1998; Joiner and da Silva 1998). The version of PSAS described in this article incorporates linear (i.e., state-independent) observation operators only. A version of the PSAS algorithm for nonlinear observation operators is described in Cohn (1997, section 5).
4) To allow maximum flexibility in forecast and observation error covariance modeling. While much effort has been directed toward covariance modeling in recent years, it is likely that additional efforts will result in improved analyses. For instance, while current global spectral variational analysis schemes rely explicitly on an assumption that forecast errors are horizontally isotropic, or on a slightly relaxed version of this assumption (Courtier et al. 1998), it is well-known (e.g., Courtier et al. 1994; Thépaut et al. 1996; Cohn and Todling 1996) that these errors are in fact highly anisotropic and flow dependent. Formulation of the analysis problem directly in physical space, rather than spectral space, renders fully anisotropic correlation modeling straightforward (e.g., Derber and Rosati 1989; Carton and Hackert 1990). The PSAS numerical algorithm makes no assumption of isotropy, although the implementation described in this article employs the isotropic correlation functions specified by the GEOS-1 OI system. Much of the current and future development is directed toward improved error correlation modeling

in PSAS (Dee and Gaspari 1996; Lou et al. 1996; Gaspari and Cohn 1998).

5) To enable flexibility for future developments in data assimilation methodology. The PSAS system was envisioned from the outset to provide a computational framework for the development of techniques for approximate fixed-lag Kalman smoothing (Todling et al. 1998; Cohn et al. 1994), approximate Kalman filtering (e.g., Cohn and Todling 1996), forecast bias estimation (Dee and da Silva 1998), and other topics known from the estimation theory literature but not yet implemented in operational data assimilation systems. Solution of the innovation covariance equation, a key component of the PSAS algorithm described below, is a need common to all of these techniques.

Because of these design features PSAS has the following attributes.

1) PSAS solves the analysis equations globally rather than locally. The local approximation and data selection of the GEOS-1 OI system are eliminated. In this respect, PSAS is similar to the global spectral variational analysis systems that have recently replaced OI schemes at the U.S. National Centers for Environmental Prediction (NCEP; Parrish and Derber 1992) and at the European Centre for Medium-Range Weather Forecasts (ECMWF; Courtier et al. 1998; Rabier et al. 1998; Andersson et al. 1998).
2) PSAS is formulated directly in physical space, like OI schemes but unlike spectral analysis schemes.
3) PSAS performs a large part of its calculations in observation space, also unlike operational spectral analysis schemes, which operate in state space. This results in computational savings, since the dimension of the observation space is currently an order of magnitude smaller than that of the forecast model state. The computational efficiency of the current generation of spectral analysis schemes arises from an assumption that horizontal forecast error covariances or correlations are either isotropic or have ellipsoidal isolines; that is, are diagonal or block-diagonal in spectral space (Courtier et al. 1998), an assumption that is not made in the PSAS algorithm.
4) PSAS is fundamentally independent of the forecast model formulation, and hence is a portable algorithm suitable for diverse applications. Although PSAS is compatible with the gridpoint system of the GEOS general circulation model, the design does not restrict PSAS applications to this grid. In particular, the PSAS algorithm is suitable for global spectral models, as well as for regional data assimilation and for problems on irregular or stretched grids such as oceanic data assimilation.

b. Background: The statistical analysis equations

A statistical analysis scheme attempts to obtain an optimal estimate, or analysis, of the state of a dynamical system by combining observations of the system with a forecast model first guess. Let $\mathbf{w}^f \in \mathcal{R}^n$ denote the vector representing the forecast first guess, defined on a grid in our case, and let $\mathbf{w}^t \in \mathcal{R}^n$ denote the discrete true state approximated by $\mathbf{w}^f$:

$$\mathbf{w}^f = \mathbf{w}^t + \boldsymbol{\epsilon}^f, \tag{1}$$

where $\boldsymbol{\epsilon}^f \in \mathcal{R}^n$ denotes the forecast error. A time index is omitted in this equation and in those to follow for notational simplicity. Let $\mathbf{w}^o \in \mathcal{R}^p$ denote the vector of p observations available at the analysis time, assumed in this article to be related linearly to the state variables:

$$\mathbf{w}^o = \mathbf{H}\mathbf{w}^t + \boldsymbol{\epsilon}^o. \tag{2}$$

Here $\mathbf{H} \in \mathcal{R}^p \times \mathcal{R}^n$ is the observation operator, or generalized interpolation operator; $\boldsymbol{\epsilon}^o \in \mathcal{R}^p$ denotes the observation error, which is the sum of the measurement error and the error of representativeness (e.g., Lorenc 1986; Cohn 1997). In the GEOS-1 DAS, the number of model degrees of freedom is $n \sim 10^6$ and the current observing system has $p \sim 10^5$.

The probabilistic assumptions common to most operational analysis systems are that $\boldsymbol{\epsilon}^f$ and $\boldsymbol{\epsilon}^o$ are Gaussian distributed with zero mean, and are not correlated with either the state or with each other. Although these assumptions can be relaxed in a variety of ways (cf. Cohn 1997 and references therein), the implementation of PSAS described in this article invokes all of them. Efforts directed toward relaxing the assumption that $\boldsymbol{\epsilon}^f$ has zero mean ($\langle \boldsymbol{\epsilon}^f \rangle = 0$), that is, that the forecast is unbiased, are described in Dee and da Silva (1998).

The two most common optimality criteria, arising from minimum variance estimation and maximum likelihood estimation, lead to identical analysis equations under these assumptions (e.g., Lorenc 1986; Cohn 1997). These equations also yield the best linear unbiased estimate, or analysis, without an assumption that the errors $\boldsymbol{\epsilon}^f$ and $\boldsymbol{\epsilon}^o$ are Gaussian distributed.

The minimum variance analysis $\mathbf{w}^a \in \mathcal{R}^n$ is obtained by requiring the scalar functional $\langle (\mathbf{w}^a - \mathbf{w}^t)^T \mathbf{S} (\mathbf{w}^a - \mathbf{w}^t) \rangle$ to be minimum for all positive definite matrices $\mathbf{S} \in \mathcal{R}^n \times \mathcal{R}^n$, and under the stated assumptions is given by the *analysis equations*:

$$\mathbf{w}^a = \mathbf{w}^f + \mathbf{K}(\mathbf{w}^o - \mathbf{H}\mathbf{w}^f) \tag{3}$$

$$\mathbf{K} = \mathbf{P}^f \mathbf{H}^T (\mathbf{H}\mathbf{P}^f \mathbf{H}^T + \mathbf{R})^{-1}. \tag{4}$$

Here the matrix $\mathbf{K} \in \mathcal{R}^n \times \mathcal{R}^p$ is the gain matrix, which ascribes appropriate weights to the observations by acting on the innovation vector[1] $\mathbf{w}^o - \mathbf{H}\mathbf{w}^f$. The gain matrix depends on the forecast error covariance matrix:

[1] Strictly speaking, the innovation vector is defined by the properties of being white in time and Gaussian with zero mean, even for nonlinear dynamics and observation operators (cf. Frost and Kailath 1971; Daley 1992). In this article we adopt the term innovation vector with the caveat that these properties are perhaps goals but not yet realities for operational data assimilation systems.

$$\mathbf{P}^f \equiv \langle(\boldsymbol{\epsilon}^f - \langle\boldsymbol{\epsilon}^f\rangle)(\boldsymbol{\epsilon}^f - \langle\boldsymbol{\epsilon}^f\rangle)^T\rangle \in \mathcal{R}^n \times \mathcal{R}^n \quad (5)$$

and on the observation error covariance matrix:

$$\mathbf{R} \equiv \langle(\boldsymbol{\epsilon}^o - \langle\boldsymbol{\epsilon}^o\rangle)(\boldsymbol{\epsilon}^o - \langle\boldsymbol{\epsilon}^o\rangle)^T\rangle \in \mathcal{R}^p \times \mathcal{R}^p. \quad (6)$$

Both are symmetric and positive semidefinite by definition; $\mathbf{R}$ is in fact positive definite under an assumption that no linear combination of the observations is perfect. Although these matrices are *defined* as above, in practice they must be modeled.

c. The global PSAS solver

The PSAS algorithm solves the analysis equations (3)–(4) in a straightforward manner. First, one $p \times p$ linear system is solved for the quantity $\mathbf{y}$,

$$(\mathbf{H}\mathbf{P}^f\mathbf{H}^T + \mathbf{R})\mathbf{y} = \mathbf{w}^o - \mathbf{H}\mathbf{w}^f, \quad (7)$$

and then the analyzed state $\mathbf{w}^a$ is obtained from the equation

$$\mathbf{w}^a = \mathbf{w}^f + \mathbf{P}^f\mathbf{H}^T\mathbf{y}. \quad (8)$$

Equations (7) and (8) will be referred to as the PSAS equations. The innovation covariance matrix:

$$\mathbf{M} \equiv \mathbf{H}\mathbf{P}^f\mathbf{H}^T + \mathbf{R} \quad (9)$$

is symmetric positive definite, making a standard preconditioned conjugate gradient (CG) algorithm (Golub and van Loan 1989) the method of choice for solving the large linear system (7), referred to as the innovation covariance equation. For the current observing system ($p \sim n/10$), setting up and solving the linear system (7) costs about half the computational effort of PSAS, and involves computation in observation space: $\mathbf{M} \in \mathcal{R}^p \times \mathcal{R}^p$ and $\mathbf{y} \in \mathcal{R}^p$, requiring $O(N_{cg}p^2)$ operations, where $N_{cg} \sim 10$ is the number of CG iterations (the convergence criterion is described later). The other half of the computational expense is taken by step (8), which transfers the solution $\mathbf{y}$ to the state space: $\mathbf{P}^f\mathbf{H}^T\mathbf{y} \in \mathcal{R}^n$, requiring $O(np)$ operations.

For typical models of $\mathbf{P}^f$ and $\mathbf{R}$ the innovation covariance matrix $\mathbf{M}$ is not sparse, although entries associated with remote pairs of observation locations are negligibly small. To introduce some sparseness in $\mathbf{M}$ and thereby to save computational effort, the sphere is divided into N regions, and matrix blocks associated with regions separated by more than 6000 km are assumed to be zero; these blocks never enter the CG computations. The same procedure is applied to the matrix $\mathbf{P}^f$ itself in (8). This is a covariance modeling assumption, rather than a local approximation like that of OI schemes, and is justified on the basis of observational studies (Hollingsworth and Lönnberg 1986; Lönnberg and Hollingsworth 1986). Although this procedure could in principle destroy the positive-definiteness of $\mathbf{M}$, causing lack of convergence of the CG solver, this has not been observed in the experiments reported in section 4 using the covariance models $\mathbf{P}^f$ and $\mathbf{R}$ of the GEOS-1 OI system. A rigorous approach based on space-limited covariance functions (Gaspari and Cohn 1998), which are exactly zero beyond a specified distance, has already been implemented in PSAS, but for the purposes of a clean comparison with the OI system is not part of the implementation described in this article.

An effective preconditioner for CG algorithms must have two important characteristics: 1) it must be inexpensive to compute, and 2) it must retain the essentials of the original matrix problem if it is to improve substantially the convergence rate of the overall CG algorithm. For the statistical interpolation problem that PSAS implements, a natural preconditioner is an OI-like approximation, in which the problem is solved separately for each of the N regions used to partition the data. For the current serial implementation, the globe is divided into $N = 80$ equal-area regions using an icosahedral grid (Pfaendtner 1996).[2] With $p \sim 100\,000$ observations, each of these regional problems has on average more than 1000 observations, which is too many for efficient direct solution. These regional problems are therefore solved by a preconditioned conjugate gradient algorithm; we refer to this solver as the *CG level 2* solver. As a preconditioner for CG level 2 the regional problems are solved univariately for each data type—that is, observations of u wind, v wind, geopotential height, etc. are treated in isolation. However, these univariate problems are still too large to be solved efficiently by direct methods, and yet another iterative solver is used; this is the *CG level 1* algorithm. As a preconditioner for CG level 1 we make use of the standard numerical linear algebra package (Anderson et al. 1992) to perform a direct Cholesky factorization of diagonal blocks of the CG level 1 matrix. These diagonal blocks are typically of size 32, and are chosen carefully to include complete vertical profiles. The overall nested preconditioned conjugate gradient algorithm is illustrated in Fig. 1. Additional details concerning this algorithm can be found in da Silva and Guo (1996).

In the serial implementation of PSAS, the matrix $\mathbf{M}$ is first normalized by its main diagonal, the normalized matrix is provided to the global CG solver as an operator, and matrix elements are recomputed at each CG iteration, as needed. In the prototype parallel implementation of PSAS developed at the Jet Propulsion Laboratory (Ding and Ferraro 1996), blocks of the matrix $\mathbf{M}$ are precomputed and stored in memory. As a convergence criterion for the global CG solver, we specify that the residual must be reduced by one to two orders of magnitude. Experiments with reduction of the resid-

[2] In the prototype massively parallel implementation of PSAS developed at the Jet Propulsion Laboratory, the globe is divided into 256 or 512 geographically irregular regions, each having approximately the same number of observations. This is one strategy to achieve load balance (Ding and Ferraro 1996).

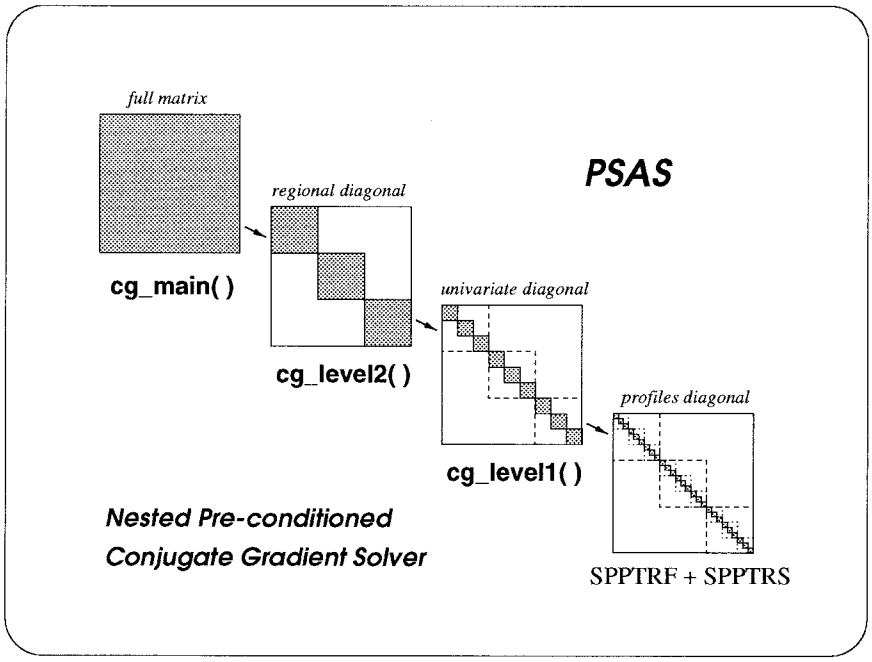

FIG. 1. PSAS nested preconditioned conjugate gradient solver. Routine cg_main( ) contains the main conjugate gradient driver. This routine is preconditioned by cg_level2( ), which solves a similar problem for each region. This routine is in turn preconditioned by cg_level1( ), which solves the linear system univariately. See text for details.

ual beyond two orders of magnitude produced differences in the resulting analyses much smaller than expected analysis errors. This is due to the filtering property of the operator $\mathbf{P}^f\mathbf{H}^T$ in (8), which attenuates small-scale details in the linear system variable **y.**

d. Relationship of PSAS, OI, and spectral variational schemes

In this section we contrast the PSAS approach to solving the analysis equations (3)–(4) with the approach of OI schemes and the approach of spectral variational schemes.

1) OPTIMAL INTERPOLATION SCHEMES

Optimal interpolation schemes solve Eqs. (3)–(4) approximately, as follows. Denote by $\mathbf{k}_j$ the jth column of the transposed gain matrix $\mathbf{K}^T$ defined by (4), so that $\mathbf{k}_j \in \mathcal{R}^p$. Then (4) can be written as

$$(\mathbf{HP}^f\mathbf{H}^T + \mathbf{R})\mathbf{k}_j = (\mathbf{HP}^f)_j \qquad (10)$$

for $j = 1, \ldots, n$, where $(\mathbf{HP}^f)_j \in \mathcal{R}^p$ denotes the jth column of the matrix $\mathbf{HP}^f$. This equation represents n linear systems, each of the same form as the PSAS equation (7). Similarly, Eq. (3) can be written as n scalar equations,

$$w_j^a = w_j^f + (\mathbf{k}_j)^T(\mathbf{w}^o - \mathbf{H}\mathbf{w}^f) \qquad (11)$$

for $j = 1, \ldots, n$, where w_j^a and w_j^f denote the jth elements of $\mathbf{w}^a$ and $\mathbf{w}^f$, respectively. This equation makes it clear that the weight vector $\mathbf{k}_j$ solved for in (10) determines the correction, or analysis increment, at the jth grid point.

Equations (10) and (11) would yield the same analysis $\mathbf{w}^a$ as the PSAS equations (7) and (8), but at far greater computational expense since there are n linear systems to be solved in (10) but only one in (7). Optimal interpolation schemes[3] do in fact solve (10) and (11), but with a local approximation and hence the need for data selection. These schemes differ widely in the details of the local approximation and the data selection algorithm (cf. McPherson et al. 1979; Lorenc 1981; Baker et al. 1987; Pfaendtner et al. 1995), but all can be described in a generic way as follows.

Instead of involving all p observations in the solution of Eqs. (10) and (11) for each j, some much smaller number of observations $q \ll p$ nearby the jth grid location is selected for the analysis at that location, and in general a different subset of observations, $q = q(j)$, is selected for different locations j. Thus $\mathbf{w}^o$, $\mathbf{H}$, and $\mathbf{R}$ become lower-dimensional and are made to depend on the gridpoint index j: $\mathbf{w}^o = \mathbf{w}_j^o \in \mathcal{R}^q$, $\mathbf{H} = \mathbf{H}_j \in \mathcal{R}^q \times$

[3] It should be noted that not all implementations of OI compute the weights $\mathbf{k}_j$ explicitly (cf. Daley 1991, section 4.2).

$\mathcal{R}^n$, and $\mathbf{R} = \mathbf{R}_j \in \mathcal{R}^q \times \mathcal{R}^q$. [This is a slight abuse of notation; for these quantities the subscript j simply denotes dependence on the gridpoint index, whereas otherwise it denotes a column of a matrix or an element of a vector.] Thus in OI schemes the analysis Eqs. (10) and (11) can be written as

$$(\mathbf{H}_j\mathbf{P}^f\mathbf{H}_j^T + \mathbf{R}_j)\mathbf{k}_j = (\mathbf{H}_j\mathbf{P}^f)_j \tag{12}$$

and

$$w_j^a = w_j^f + (\mathbf{k}_j)^T(\mathbf{w}_j^o - \mathbf{H}_j\mathbf{w}^f) \tag{13}$$

for $j = 1, \ldots, n$, where now $\mathbf{k}_j \in \mathcal{R}^q$. Although there are still n systems to solve in (12), each is now only $q \times q$ (this is the local approximation), and q is made small enough that a direct method such as the standard Cholesky algorithm can be used to solve them. In addition, for *volume* OI methods (Lorenc 1981; Pfaendtner et al. 1995), the matrix $\mathbf{M}_j = \mathbf{H}_j\mathbf{P}^f\mathbf{H}_j^T + \mathbf{R}_j$ in (12) is fixed for a given volume, so that the Cholesky decomposition can be reused for each grid point in that volume, reducing computational effort.

2) Spectral variational schemes

Variational analysis schemes are based on the maximum likelihood optimality criterion which, under the probabilistic assumptions noted above Eq. (3), is identical to the minimum variance criterion, and hence leads to a formulation of the analysis problem that is algebraically equivalent to that of PSAS. The actual equations solved by these schemes, however, are different from those of PSAS.

The maximum likelihood criterion seeks to maximize the a posteriori (conditional) probability density $p(\mathbf{w}^t|\mathbf{w}^f, \mathbf{w}^o)$, which under the stated assumptions is the Gaussian density

$$p(\mathbf{w}^t|\mathbf{w}^f, \mathbf{w}^o) = c\,\exp[-\tilde{J}(\mathbf{w}^t)], \tag{14}$$

where

$$c = (2\pi)^{-n/2}|\mathbf{R}|^{-1/2}|\mathbf{P}^f|^{-1/2}|\mathbf{H}\mathbf{P}^f\mathbf{H}^T + \mathbf{R}|^{1/2}, \tag{15}$$

the symbol $|\cdot|$ denoting the matrix determinant, and where

$$\begin{aligned}\tilde{J}(\mathbf{w}^t) = {} & \frac{1}{2}(\mathbf{w}^t - \mathbf{w}^f)^T(\mathbf{P}^f)^{-1}(\mathbf{w}^t - \mathbf{w}^f) \\ & + \frac{1}{2}(\mathbf{H}\mathbf{w}^t - \mathbf{w}^o)^T\mathbf{R}^{-1}(\mathbf{H}\mathbf{w}^t - \mathbf{w}^o) \\ & - \frac{1}{2}(\mathbf{w}^o - \mathbf{H}\mathbf{w}^f)^T(\mathbf{H}\mathbf{P}^f\mathbf{H}^T + \mathbf{R})^{-1}(\mathbf{w}^o - \mathbf{H}\mathbf{w}^f);\end{aligned} \tag{16}$$

compare Jazwinski (1970, section 7.2), Lorenc (1986), Cohn (1997, section 4). Since the constant c is independent of $\mathbf{w}^t$, as is the final term in (16), and since $\exp(-\tilde{J})$ is a monotonically decreasing function of $\tilde{J}$, maximizing the density (14) with respect to $\mathbf{w}^t$ is equivalent to minimizing with respect to $\mathbf{w}$ the functional

$$\begin{aligned}J(\mathbf{w}) = {} & \frac{1}{2}(\mathbf{w} - \mathbf{w}^f)^T(\mathbf{P}^f)^{-1}(\mathbf{w} - \mathbf{w}^f) \\ & + \frac{1}{2}(\mathbf{H}\mathbf{w} - \mathbf{w}^o)^T\mathbf{R}^{-1}(\mathbf{H}\mathbf{w} - \mathbf{w}^o).\end{aligned} \tag{17}$$

Since this functional is a positive definite quadratic form in $\mathbf{w}$, it has a unique minimum. This minimum is denoted by $\mathbf{w}^a$, the analysis vector. Variational analysis schemes are so called because they take minimization of (17), or of a similar functional, as the starting point.

Details of the minimization procedure differ between the two operational implementations to date, namely the 3D-Var (three-dimensional variational) system of ECMWF (Courtier et al. 1998; Rabier et al. 1998; Andersson et al. 1998), which became operational in early 1996, and the spectral statistical interpolation (SSI) system of NCEP (Parrish and Derber 1992; hereafter referred to as PD92), which became operational in early 1992. Here we follow PD92. Setting

$$\left.\frac{\partial J(\mathbf{w})}{\partial \mathbf{w}}\right|_{\mathbf{w}=\mathbf{w}^a} = 0 \tag{18}$$

gives the equation

$$[(\mathbf{P}^f)^{-1} + \mathbf{H}^T\mathbf{R}^{-1}\mathbf{H}](\mathbf{w}^a - \mathbf{w}^f) = \mathbf{H}^T\mathbf{R}^{-1}(\mathbf{w}^o - \mathbf{H}\mathbf{w}^f). \tag{19}$$

Now let B be any matrix such that

$$\mathbf{B}\mathbf{B}^T = \mathbf{P}^f \tag{20}$$

(this decomposition, carried out spectrally, is discussed later), and define the vector $\mathbf{z} \in \mathcal{R}^n$ such that

$$\mathbf{z} = \mathbf{B}^{-1}(\mathbf{w}^a - \mathbf{w}^f). \tag{21}$$

Algebraic manipulation of (19) leads to the equation

$$(\mathbf{I} + \mathbf{B}^T\mathbf{H}^T\mathbf{R}^{-1}\mathbf{H}\mathbf{B})\mathbf{z} = \mathbf{B}^T\mathbf{H}^T\mathbf{R}^{-1}(\mathbf{w}^o - \mathbf{H}\mathbf{w}^f), \tag{22}$$

which along with (21) written in the form

$$\mathbf{w}^a = \mathbf{w}^f + \mathbf{B}\mathbf{z}, \tag{23}$$

compose the analysis equations of PD92. These can be compared directly with the PSAS analysis equations (7) and (8). Observe that (22) is an equation solved in state space—that is, $\mathbf{z} \in \mathcal{R}^n$—whereas the matrix problem (7) of PSAS is solved in the lower-dimensional observation space $\mathcal{R}^p$. Solving (22) involves additionally the solution of observation-space systems of the form $\mathbf{R}\mathbf{u} = \mathbf{v}$.

To establish the equivalence of the analysis equations of PD92 with those of PSAS when presented with the same data $\mathbf{w}^o$, $\mathbf{w}^f$, and the same matrices $\mathbf{P}^f$, $\mathbf{R}$ and $\mathbf{H}$, note from the Sherman–Morrison–Woodbury formula (e.g., Golub and van Loan 1989) that

$$(\mathbf{I} + \mathbf{B}^T\mathbf{H}^T\mathbf{R}^{-1}\mathbf{H}\mathbf{B})^{-1} = \mathbf{I} - \mathbf{B}^T\mathbf{H}^T(\mathbf{H}\mathbf{P}^f\mathbf{H}^T + \mathbf{R})^{-1}\mathbf{H}\mathbf{B}, \tag{24}$$

so that (22) can be written as

$$\begin{aligned}\mathbf{Bz} &= \mathbf{B}[\mathbf{I} - \mathbf{B}^T\mathbf{H}^T(\mathbf{H}\mathbf{P}^f\mathbf{H}^T + \mathbf{R})^{-1}\mathbf{H}\mathbf{B}]\mathbf{B}^T\mathbf{H}^T\mathbf{R}^{-1}(\mathbf{w}^o - \mathbf{H}\mathbf{w}^f)\\ &= \mathbf{P}^f\mathbf{H}^T[\mathbf{I} - (\mathbf{H}\mathbf{P}^f\mathbf{H}^T + \mathbf{R})^{-1}\mathbf{H}\mathbf{P}^f\mathbf{H}^T]\mathbf{R}^{-1}(\mathbf{w}^o - \mathbf{H}\mathbf{w}^f)\\ &= \mathbf{P}^f\mathbf{H}^T(\mathbf{H}\mathbf{P}^f\mathbf{H}^T + \mathbf{R})^{-1}(\mathbf{w}^o - \mathbf{H}\mathbf{w}^f)\\ &= \mathbf{P}^f\mathbf{H}^T\mathbf{y}, \end{aligned} \tag{25}$$

where $\mathbf{y}$ was defined by the PSAS equation (7). This result, along with (8) and (23), establishes the formal algebraic equivalence between the SSI scheme of PD92 and the PSAS scheme (see also Lorenc 1986; Courtier 1997). The differences, therefore, are in the solution algorithm and, perhaps more importantly, in the covariance modeling. The matrix $\mathbf{P}^f$ is modeled directly in physical space in PSAS, whereas in variational schemes such as SSI it is modeled spectrally.

In the SSI scheme, as well as in the 3D-Var scheme of ECMWF, the forecast $\mathbf{w}^f$, and hence the true state $\mathbf{w}^t$ and the analysis $\mathbf{w}^a$, consists of spectral coefficients rather than gridpoint values as in the GEOS system. Thus the observation operator $\mathbf{H}$ in (22) consists of a transformation to physical space followed by interpolation to observation locations [see Eq. (2)], which, as reported in PD92, composes most of the computational effort in solving (22). The spectral forecast error covariance matrix $\mathbf{P}^f$, still defined by (5), is assumed to be diagonal. This renders the decomposition (20) trivial, but is an explicit assumption of horizontal isotropy. In particular, the wind forecast error variances of PD92 are independent of horizontal location. The ECMWF 3D-Var system assumes isotropy for horizontal correlations rather than covariances, thereby allowing spatial variability in the forecast error variances (Courtier et al. 1998).

The linear system (22) of PD92 is solved by a standard CG algorithm without preconditioning; this is equivalent computationally to solving (19) by a preconditioned CG algorithm with the (diagonal) matrix $\mathbf{P}^f$ as the preconditioner, as is done in the ECMWF 3D-Var system (Courtier et al. 1998). The eigenvalues μ of the matrix of the linear system (22) have the form

$$\mu = 1 + \lambda(\tilde{\mathbf{M}}), \tag{26}$$

where

$$\tilde{\mathbf{M}} \equiv \mathbf{B}^T\mathbf{H}^T\mathbf{R}^{-1}\mathbf{H}\mathbf{B}, \tag{27}$$

and $\lambda(\tilde{\mathbf{M}})$ denotes an eigenvalue of the matrix $\tilde{\mathbf{M}}$. The matrix $\tilde{\mathbf{M}}$ is symmetric positive semidefinite, and has at least $n - p$ zero eigenvalues, assuming $p < n$. Thus the condition number σ of the matrix of (22), which controls the convergence rate of the CG algorithm (cf. Golub and van Loan 1989), is

$$\sigma = 1 + \lambda_{\max}(\tilde{\mathbf{M}}). \tag{28}$$

Accurate observational data (reflected by small diagonal entries of $\mathbf{R}$) generally increase the largest eigenvalue $\lambda_{\max}(\tilde{\mathbf{M}})$ according to (27), and therefore increase the condition number σ and generally reduce the convergence rate of the CG iterations. It can be shown that, were the PSAS equation (7) to be preconditioned by the matrix $\mathbf{R}$ rather than by the strategy described in the preceding subsection, its condition number would also be given by (28); compare Courtier (1997).

3. GEOS-1 DAS: An OI-based data assimilation system

Version 1 of the Goddard Earth Observing System Data Assimilation System (GEOS-1 DAS) has two main components: a gridpoint atmospheric general circulation model and an OI analysis system. These two components are described briefly below. Data quality control routines are described in Pfaendtner et al. (1995). Analysis increments are assimilated into the model using the Incremental Analysis Updates (IAU) technique of Bloom et al. (1996); IAU effectively removes the need for initialization.

a. The GEOS-1 general circulation model

A detailed documentation of this model can be found in Takacs et al. (1995). The main characteristics of this primitive equation model are the following:

- *Resolution*: 2° lat × 2.5° long, 20 sigma levels.
- *Spatial discretization*: Potential enstrophy- and energy-conserving horizontal differencing scheme on a C-grid (Sadourny 1975); vertical discretization of Arakawa and Suarez (1983).
- *Time stepping*: Matsuno during assimilation mode; leapfrog with Asselin–Robert time filter (Asselin 1972) in pure forecast mode.
- *Convection*: Relaxed Arakawa–Schubert (Moorthi and Suarez 1992); large-scale convection (Sud and Molod 1988).
- *Radiation*: Longwave and shortwave parameterizations (see Takacs et al. 1995 for details).
- *Turbulence*: Second-order closure model of Helfand and Labraga (1988); Monin–Obukhov similarity theory for the surface layer.
- *Boundary conditions*: Observed monthly mean sea surface temperature (NCEP); soil moisture computed off-line based on a simple bucket model (Schemm et al. 1992).

b. The GEOS-1 OI analysis system

An early version of this system was described by Baker et al. (1987); the GEOS-1 version is documented in Pfaendtner et al. (1995). The main features of this system include the following:

- *Resolution*: 2° lat × 2.5° long, 14 upper-air pressure levels (20, 30, 50, 70, 100, 150, 200, 250, 300, 400, 500, 700, 850, and 1000 hPa). The transformation between the analysis coordinate (pressure), on which the forecast error statistics are prescribed, and the model coordinate (sigma) is described in Pfaendtner et al. (1995), as is the transformation between analysis variables (geopotential height, wind, water vapor mixing ratio, sea level pressure) and model variables (potential temperature, wind, specific humidity, surface pressure).
- *Forecast error statistics*: Multivariate in geopotential height and winds, univariate in moisture. The height forecast error correlation function is separable, with a damped cosine function for the isotropic horizontal correlation. The wind/height and wind/wind error correlation functions are derived from the height error correlation function under the geostrophic assumption, with full coupling in the extratropics and the coupling coefficient approaching zero at the equator. Forecast error variances for height, moisture, and sea level pressure are obtained from analysis error variances calculated approximately at the previous analysis time, through a growth term depending on latitude, pressure level, and saturation value.
- *Surface analysis*: Decoupled from the upper-air analysis. Sea level pressure and surface wind statistics are coupled through a frictional-wind balance. The sea level pressure analysis is used to translate satellite-derived thicknesses into heights and also to provide 1000-hPa pseudoheights for the upper-air analysis.
- *Data sources*: All conventional meteorological data including rawinsondes, dropwinsondes, rocketsondes, aircraft winds, satellite-tracked winds, and thicknesses from *TIROS-N* Operational Vertical Sounder (TOVS) soundings.
- *Analysis frequency*: Four times per day, using observations within a 6-h window centered at the synoptic times. The innovation vector is calculated from a single forecast valid at the synoptic time.
- *Local approximation/data selection*: Volume method of Lorenc (1981), with approximately 12 000 overlapping volumes. The horizontal extent of each volume depends on latitude. In the vertical, each volume consists of two adjacent pressure levels. Data are selected from these two levels and also one level above (except for the 20–30-hPa analysis) and one level below (except for the 850–1000-hPa analysis). At most 75 observations are selected from within a 1600-km radius of the center of each volume.

TABLE 1. Five synoptically interesting cases used in this study. For all cases the synoptic time is 1200 UTC.

Case	Date	Description
1	08/28/85	Tropical easterly waves
2	10/15/87	Explosive cyclogenesis (Europe)
3	12/01/87	Cyclogenesis (south Australia)
4	12/15/87	Explosive cyclogenesis (United States)
5	01/30/89	Cold surge (United States)

4. Comparison of the global PSAS solver with the local OI solver

To isolate the effects of localization of the analysis problem in the GEOS-1 OI system, in the initial implementation of PSAS the forecast and observation error covariance statistics are specified in exactly the same way as in the OI system. In this configuration, PSAS differs from OI only in the numerical method used to solve for the analysis increments $\mathbf{w}^a - \mathbf{w}^f$: the global conjugate gradient solver includes all available observations to produce the analyzed field. Here we report results of a set of static analysis experiments and of a 1-month assimilation experiment comparing PSAS analyses with those of the OI system. Identical quality-controlled observational data are used in each comparison.

a. Static analysis experiments

For the static analysis experiments, we rely on the database prepared through the GEOS-1 reanalysis project described in Schubert et al. (1993). This data bank provides not only the analysis increments produced by the OI-based assimilation system, but also the innovation vectors used by the OI system (before data selection and after quality control), which are used for the rhs of (7) in the present study. A number of synoptically interesting events were identified by R. Atlas and J. C. Jusem (1996, personal communication) for the purpose of these experiments. The five cases selected are summarized in Table 1. For each case, a single PSAS analysis is carried out at 1200 UTC and results are compared with the corresponding OI analyses.

For this comparison we chose to include only data on the same vertical levels as in the OI system, thus focusing on horizontal aspects of localization in the OI system. Thus for the 500-hPa analyses compared here, only data from 850 hPa to 400 hPa are included. For the 200-hPa analyses, only data from 300 hPa to 150 hPa are used. The OI system *selects* data from these levels, whereas the PSAS solver uses all data on these levels.

Midtropospheric (500 hPa) height analysis increments for case 1 are shown in Fig. 2. The same large-scale features are present in both panels, with the OI analysis increments (bottom panel) showing the typical boxiness effect associated with the local approximation. Results for all five cases are summarized in Fig. 3, which depicts the five-case average power spectra of 500-hPa

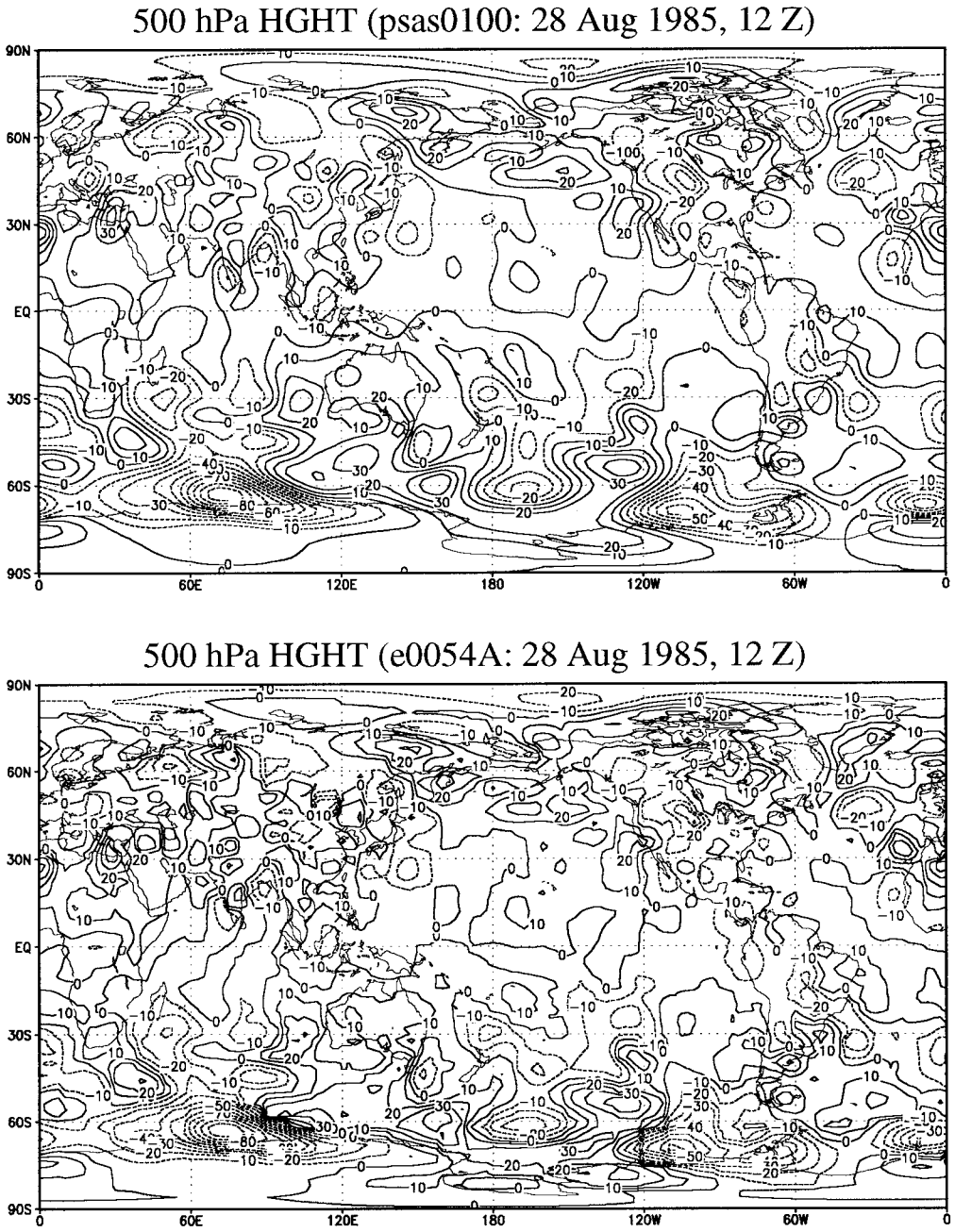

FIG. 2. Height analysis increments at 500 hPa for 1200 UTC 28 August 1985 (case 1) produced with PSAS (top panel) and GEOS-1 OI (bottom panel). Contour interval: 10 m.

geopotential height analysis increments obtained with the PSAS (solid line) and OI (dashed line) systems. There is little difference between the spectra for wavenumbers in the range 5–15. For higher wavenumbers, however, the OI analysis increments have considerably more power than the PSAS increments, apparently at the expense of a loss of power for wavenumbers less than about 5, where the OI increments have significantly less power than the PSAS increments (note the logarithmic scale in Fig. 3). The relatively flat spectral slope of the OI increments, manifested in the boxiness of Fig. 2, is a shortcoming due to the local manner in which the OI increments are calculated. Notice that the PSAS increments also show signs of saturation at around wavenumber 70. However, there is a negligible amount of power at these wavenumbers.

The effect of localization on the wind field is presented in Figs. 4–5 in terms of the five-case average

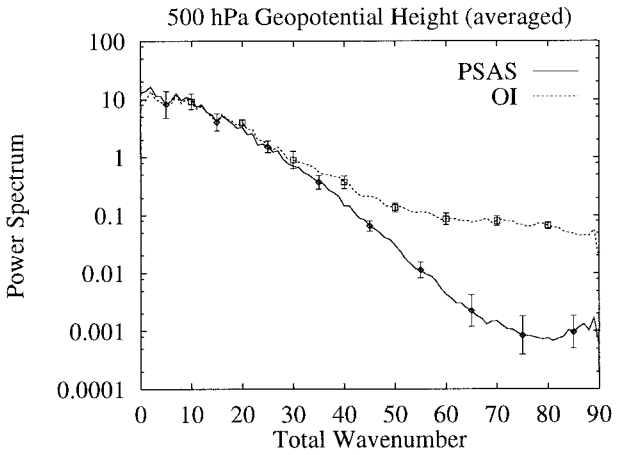

FIG. 3. Power spectra as a function of spherical harmonic total wavenumber for PSAS (solid line) and OI (dashed line) analysis increments of geopotential height at 500 hPa (five-case average, see Table 1). Bars indicate the range of the spectra among the five cases. Units: m^2.

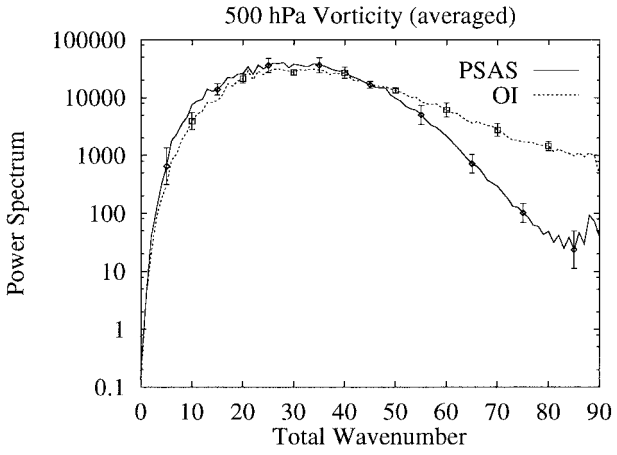

FIG. 4. As in Fig. 3 but for 500-hPa relative vorticity. Units: 10^{-15} s^{-2}.

power spectra of relative vorticity and divergence analysis increments. The OI relative vorticity analysis increments show less power than the PSAS increments up to about wavenumber 45 (Fig. 4). At higher wavenumbers the OI increments again show much more power than the PSAS increments. For the divergence field (Fig. 5), both the OI and PSAS increments show a rather flat spectrum for wavenumbers greater than about 20. For wavenumbers beyond 20 the OI increments have one to two orders of magnitude more power than the PSAS increments. Thus the ratio of divergence to vorticity for the OI increments is much larger than for the PSAS increments. This unrealistically large amount of divergence in the OI increments contributes to an unbalanced analyzed state contaminated by gravity waves. Therefore the imbalances found in GEOS-1 OI analyses (Bloom et al. 1996), although ameliorated by the IAU procedure, are due not only to the crude geostrophic balance used to relate wind forecast error statistics to height forecast error statistics: a great deal of spurious divergence is due to the local nature of the OI calculations. In addition, there is little correspondence between the spatial patterns of OI and PSAS velocity potential analysis increments, even at large scales, as can be seen in Fig. 6.

In the power spectra of water vapor mixing ratio analysis increments for OI and PSAS (not shown), the OI increments again have more noise, reflected by excessive power in higher wavenumbers. Although similar to the power spectra of geopotential height analysis increments, the discrepancy between OI and PSAS is not as accentuated in this case. This result is consistent with the shorter horizontal correlation length assigned to the water vapor mixing ratio forecast error covariance function. The tighter function for water vapor mixing ratio is more amenable to the local approximation of the OI system.

b. Assimilation experiment

For this experiment, a version of the GEOS DAS was configured using a 46-level version of the GEOS-1 general circulation model, and PSAS with the error statistics of the GEOS-1 OI system. For computational efficiency in the PSAS solver, TOVS satellite retrievals within a radius of 300 km were averaged to produce super-observations, following Lorenc (1981).

Figure 7 depicts the time-mean bias and standard deviation (Stdv) of radiosonde observation minus 6-h forecast residuals (innovations) for the last 10 days of 1-month (February 1992) assimilations with PSAS and with the GEOS-1 OI system. For geopotential height (left panel), PSAS shows a slight increase over OI in the bias in the troposphere, but a decrease above 100 hPa; standard deviations are practically the same for

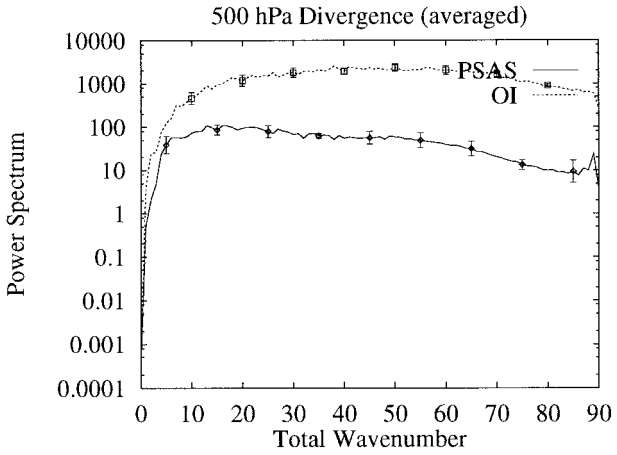

FIG. 5. As in Fig. 3 but for 500-hPa divergence. Units: 10^{-15} s^{-2}.

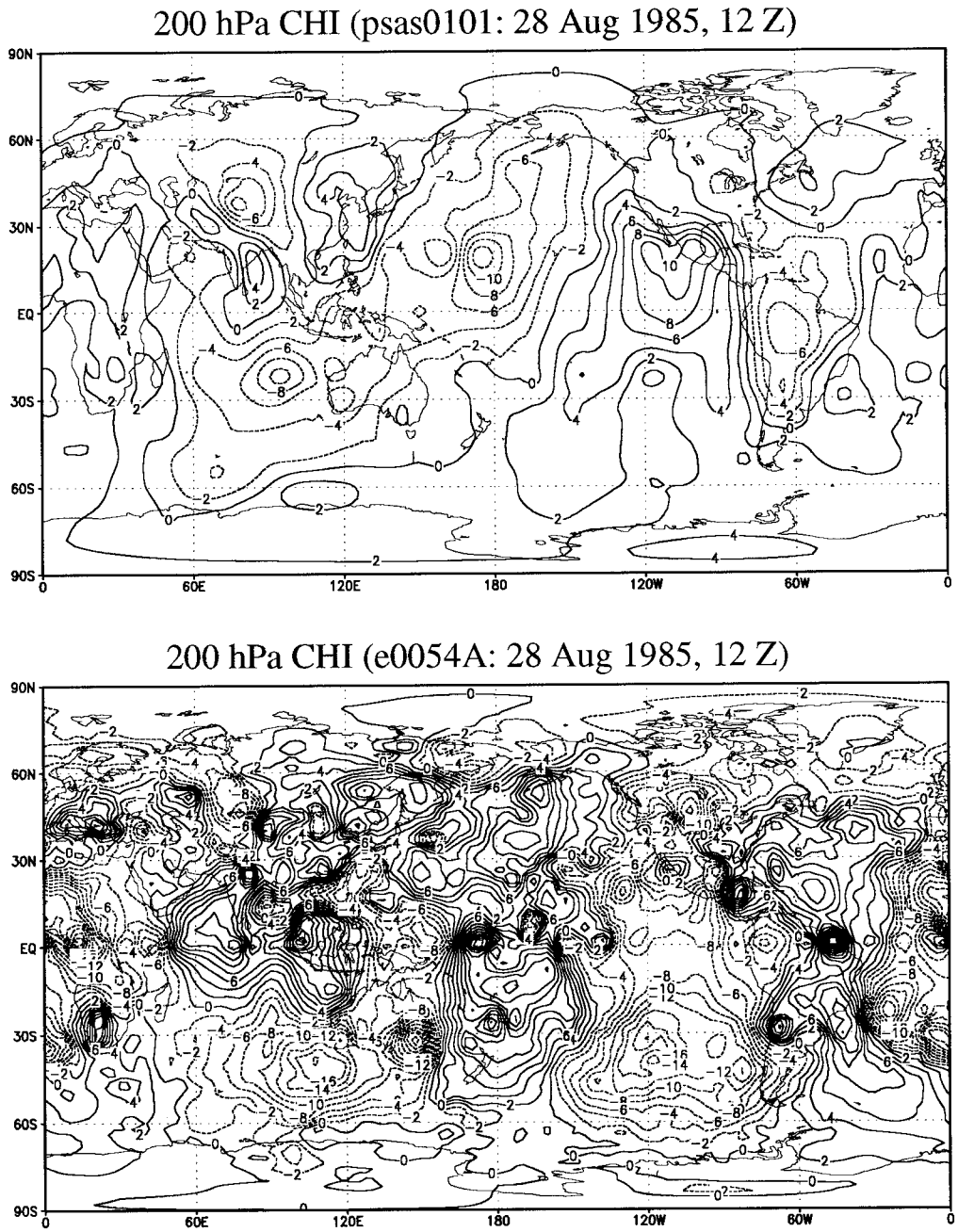

FIG. 6. Velocity potential analysis increments at 200 hPa for 1200 UTC 28 August 1985 (case 1) produced with PSAS (top panel) and GEOS-1 OI (bottom panel). Normalization is by the factor ($2\Omega \sin 45^\circ\, g^{-1}$), where Ω is the earth's rotation rate and g is the gravity constant. Contour interval: 2 m.

both systems. For the zonal component of the wind (right panel), PSAS shows a slight improvement in the bias, and a substantial improvement in the standard deviation below 200 hPa and above 40 hPa. Statistics for water vapor mixing ratio (not shown) are nearly identical for both systems. These results are consistent with the analysis increment characteristics displayed in Figs. 3–5. Whereas the noise introduced by the local nature of OI is filtered effectively by the IAU procedure (Bloom et al. 1996), the dynamical imbalance associated with the spurious OI analysis increments of divergence have a deleterious effect on the 6-h wind forecast.

5. Concluding remarks

We have described the mathematical formulation and algorithmic design of the Physical-space Statistical Analysis System. This formulation has been contrasted

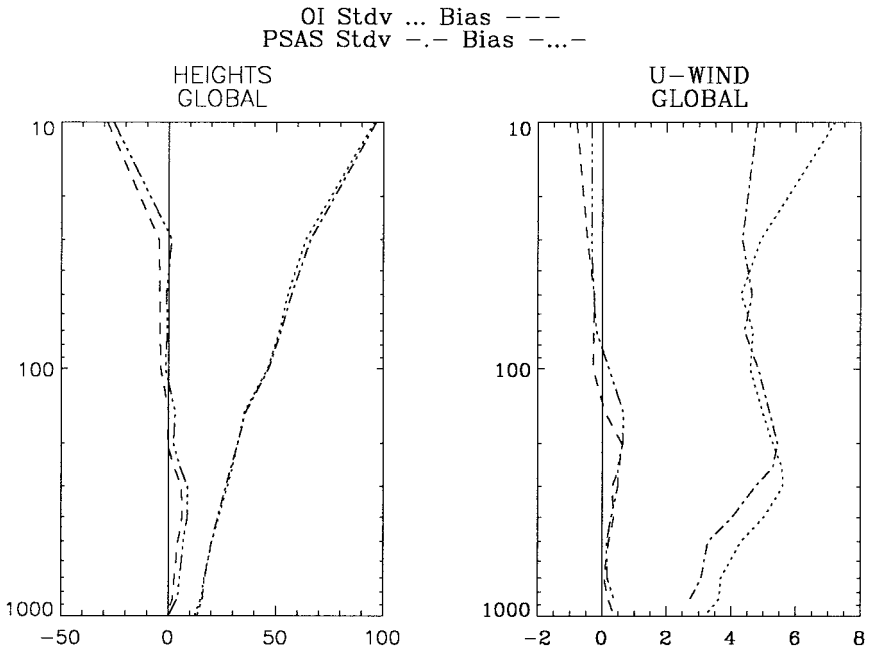

FIG. 7. Time-mean bias and standard deviation of radiosonde observation minus 6-h forecast residuals for geopotential height (left panel, units: m) and for the zonal wind component (right panel, units: m s^{-1}).

with that of optimal interpolation (OI) schemes and of spectral variational analysis schemes. It has been shown to be algebraically equivalent to spectral variational schemes for linear observation operators, when presented with the same data and the same error covariance models. Like spectral variational schemes, PSAS circumvents the need for data selection, an ad hoc procedure required in OI schemes, by solving the analysis problem globally rather than locally. This is accomplished in the PSAS algorithm by employing a global conjugate gradient solver, preconditioned by a series of smaller OI-like problems.

Because of its formulation directly in physical space, the PSAS algorithm allows for flexible specification of error covariance models, such as flow-dependent, fully anisotropic ones, whereas current spectral variational schemes make an explicit assumption of isotropy or weak anisotropy. The only covariance modeling assumption made in the PSAS algorithm is that forecast and observation error covariances are exactly zero beyond 6000 km, an approximation supported by observational studies. While the initial implementation of PSAS described in this article purposely employs the separable, isotropic covariance models of the GEOS-1 OI system, and is therefore not yet a stand-alone analysis system, work is currently in progress to exploit the flexibility of PSAS to incorporate much more general covariance models.

By implementing PSAS with covariance models identical to those of the GEOS-1 OI system, we have been able to examine in isolation the effects of global versus local solution of the analysis problem in an operational data assimilation system. Results show that, relative to the PSAS analysis increments, the OI analysis increments of geopotential height have excessive power in small scales, apparently at the expense of too little power in large scales. The OI increments also display an unrealistically large ratio of divergence to vorticity, resulting in an unbalanced analyzed state. Time-mean radiosonde minus 6-h forecast statistics are comparable for the two systems in terms of bias, whereas the PSAS system shows a significant reduction in the standard deviation of the zonal wind component throughout the troposphere and in much of the stratosphere.

Acknowledgments. We would like to thank R. Rood and F. Einaudi for their patient, unfailing support during the course of this work. We also thank R. Atlas and J. C. Jusem for kindly providing the case selection used in this study. Insightful discussions with J. Stobie and M. Seablom are gratefully acknowledged. Helpful reviews of the manuscript were provided by P. Lyster and by two anonymous referees. The research and development documented in this article were supported by the NASA EOS Interdisciplinary Science Program and by the NASA Research and Applications Program. Computer resources and funding were provided by the EOS Program through the Data Assimilation Office. Preliminary results of this research were presented at the Second International Symposium on Assimilation of

Observations in Meteorology and Oceanography, Tokyo, 13–17 March 1995.

REFERENCES

Anderson, E., and Coauthors, 1992: *LAPACK Users' Guide.* Society for Industrial and Applied Mathematics, 235 pp.

Andersson, E., and Coauthors, 1998: The ECMWF implementation of three dimensional variational assimilation (3D-VAR). Part III: Experimental results. *Quart. J. Roy. Meteor. Soc.,* **124,** 1831–1860.

Arakawa, A., and M. J. Suarez, 1983: Vertical differencing of the primitive equations in sigma coordinates. *Mon. Wea. Rev.,* **111,** 34–45.

Asselin, R., 1972: Frequency filter for time integrations. *Mon. Wea. Rev.,* **100,** 487–490.

Baker, W. E., S. C. Bloom, J. S. Woollen, M. S. Nestler, E. Brin, T. W. Schlatter, and G. W. Branstator, 1987: Experiments with a three-dimensional statistical objective analysis scheme using FGGE data. *Mon. Wea. Rev.,* **115,** 273–296.

Bergman, K. H., 1979: Multivariate analysis of temperatures and winds using optimum interpolation. *Mon. Wea. Rev.,* **107,** 1423–1444.

Bloom, S. C., L. L. Takacs, A. M. da Silva, and D. Ledvina, 1996: Data assimilation using incremental analysis updates. *Mon. Wea. Rev.,* **124,** 1256–1271.

Carton, J. A., and E. C. Hackert, 1990: Data assimilation applied to the temperature and circulation in the tropical Atlantic. *J. Phys. Oceanogr.,* **20,** 1150–1165.

Cohn, S. E., 1997: An introduction to estimation theory. *J. Meteor. Soc. Japan,* **75,** 257–288.

——, and R. Todling, 1996: Approximate data assimilation schemes for stable and unstable dynamics. *J. Meteor. Soc. Japan,* **74,** 63–75.

——, N. S. Sivakumaran, and R. Todling, 1994: A fixed-lag Kalman smoother for retrospective data assimilation. *Mon. Wea. Rev.,* **122,** 2838–2867.

Courtier, P., 1997: Dual formulation of four-dimensional variational assimilation. *Quart. J. Roy. Meteor. Soc.,* **123,** 2449–2461.

——, J.-N. Thépaut, and A. Hollingsworth, 1994: A strategy for operational implementation of 4D-Var, using an incremental approach. *Quart. J. Roy. Meteor. Soc.,* **120,** 1367–1388.

——, and Coauthors, 1998: The ECMWF implementation of three dimensional variational assimilation (3D-VAR). Part I: Formulation. *Quart. J. Roy. Meteor. Soc.,* **124,** 1783–1808.

Daley, R., 1991: *Atmospheric Data Analysis.* Cambridge University Press, 457 pp.

——, 1992: The lagged innovation covariance: A performance diagnostic for atmospheric data assimilation. *Mon. Wea. Rev.,* **120,** 178–196.

da Silva, A., and J. Guo, 1996: Documentation of the Physical-Space Statistical Analysis System (PSAS) Part I: The Conjugate Gradient Solver Version PSAS-1.00. DAO Office Note 96-02, 66 pp. [Available from Data Assimilation Office, Goddard Space Flight Center, Greenbelt, MD 20771, and online at http://dao.gsfc.nasa.gov/subpages/office-notes.html.]

Dee, D., and G. Gaspari, 1996: Development of anisotropic correlation models for atmospheric data assimilation. Preprints, *11th Conf. on Numerical Weather Prediction,* Norfolk, VA, Amer. Meteor. Soc., 249–251.

——, and A. M. da Silva, 1998: Data assimilation in the presence of forecast bias. *Quart. J. Roy. Meteor. Soc.,* **124,** 269–295.

Derber, J., and A. Rosati, 1989: A global oceanic data assimilation system. *J. Phys. Oceanogr.,* **19,** 1333–1347.

——, and W.-S. Wu, 1998: The use of toys cloud-cleared radiances in the NCEP SSI analysis system. *Mon. Wea. Rev.,* **126,** 2287–2299.

Ding, H. D., and R. D. Ferraro, 1996: A parallel climate data assimilation package. *SIAM News,* **29,** 1–11.

Eyre, J. R., A. P. Kelly, A. P. McNally, E. Andersson, and A. Persson, 1993: Assimilation of TOVS radiance information through one-dimensional variational analysis. *Quart. J. Roy. Meteor. Soc.,* **119,** 1427–1463.

Frost, P. A., and T. Kailath, 1971: An innovations approach to least-squares estimation. Part III: Nonlinear estimation in white Gaussian noise. *IEEE Trans. Automat. Contr.,* **16,** 217–226.

Gaspari, G., and S. E. Cohn, 1998: Construction of correlation functions in two and three dimensions. DAO Office Note 96-03RI, 53 pp. [Available from Data Assimilation Office, Goddard Space Flight Center, Greenbelt, MD 20771, and online at http://dao.gsfc.nasa.gov/subpages/office-notes.html.]

Golub, G. H., and C. F. van Loan, 1989: *Matrix Computations.* 2d ed. The John Hopkins University Press, 642 pp.

Helfand, H. M., and J. C. Labraga, 1988: Design of a non-singular level 2.5 second-order closure model for the prediction of atmospheric turbulence. *J. Atmos. Sci.,* **45,** 113–132.

Hollingsworth, A., and P. Lönnberg, 1986: The statistical structure of short range forecast errors as determined from radiosonde data. Part I: The wind errors. *Tellus,* **38A,** 111–136.

Jazwinski, A. H., 1970: *Stochastic Processes and Filtering Theory.* Academic Press, 376 pp.

Joiner, J., and A. M. da Silva, 1998: Efficient methods to assimilate satellite retrievals based on information content. *Quart. J. Roy. Meteor. Soc.,* **124,** 1669–1694.

Ledvina, D. V., and J. Pfaendtner, 1995: Inclusion of Special Sensor Microwave/Imager (SSM/I) total precipitable water estimates into the GEOS-1 data assimilation system. *Mon. Wea. Rev.,* **123,** 3003–3015.

Lönnberg, P., and A. Hollingsworth, 1986: The statistical structure of short range forecast errors as determined from radiosonde data. Part II: Covariance of height and wind errors. *Tellus,* **38A,** 137–161.

Lorenc, A. C., 1981: A global three-dimensional multivariate statistical interpolation scheme. *Mon. Wea. Rev.,* **109,** 701–721.

——, 1986: Analysis methods for numerical weather prediction. *Quart. J. Roy. Meteor. Soc.,* **112,** 1177–1194.

Lou, G.-P., A. da Silva, D. Dee, and C. Redder, 1996: Modeling fully anisotropic wind/mass error covariances in physical-space. Preprints, *11th Conf. on Numerical Weather Prediction,* Norfolk, VA, Amer. Meteor. Soc., 253.

McPherson, R. D., K. H. Bergman, R. E. Kistler, G. E. Rasch, and D. S. Gordon, 1979: The NMC operational global data assimilation system. *Mon. Wea. Rev.,* **107,** 1445–1461.

Moorthi, S., and M. J. Suarez, 1992: Relaxed Arakawa–Schubert: A parameterization of moist convection for general circulation models. *Mon. Wea. Rev.,* **120,** 978–1002.

Parrish, D. F., and J. C. Derber, 1992: The National Meteorological Center's spectral statistical-interpolation analysis system. *Mon. Wea. Rev.,* **120,** 1747–1763.

Pfaendtner, J., 1996: Notes on the icosahedral domain decomposition in PSAS. DAO Office Note 96-04, 5 pp. [Available from Data Assimilation Office, Goddard Space Flight Center, Greenbelt, MD 20771, and online at http://dao.gsfc.nasa.gov/subpages/office-notes.html.]

——, S. Bloom, D. Lamich, M. Seablom, M. Sienkiewicz, J. Stobie, and A. da Silva, 1995: Documentation of the Goddard Earth Observing System (GEOS) Data Assimilation System-Version 1. NASA Tech. Memo. 104606, Vol. 4, 44 pp. [Available from NASA Goddard Space Flight Center, Greenbelt, MD 20771, and online at http://dao.gsfc.nasa.gov/subpages/tech-reports.html.]

Rabier, F., A. Mc Nally, E. Andersson, P. Courtier, P. Undén, J. Eyre, A. Hollingsworth, and F. Bouttier, 1998: The ECMWF implementation of three dimensional variational assimilation (3D-VAR). Part II: Structure functions. *Quart. J. Roy. Meteor. Soc.,* **124,** 1809–1830.

Sadourny, R., 1975: The dynamics of finite difference models of the shallow water equations. *J. Atmos. Sci.,* **32,** 680–689.

Schemm, J., S. Schubert, J. Terry, and S. Bloom, 1992: Estimates of monthly mean soil moisture for 1979–1989. NASA Tech. Memo. No. 104571, 252 pp. [Available from NASA/Goddard Space Flight Center, Greenbelt, MD 20771.]

Schubert, S. D., J. Pfaendtner, and R. Rood, 1993: An assimilated data set for earth science applications. *Bull. Amer. Meteor. Soc.,* **74,** 2331–2342.

Sud, Y. C., and A. Molod, 1988: The roles of dry convection, cloud-radiation feedback processes and the influence of recent improvements in the parameterization of convection in the GLA GCM. *Mon. Wea. Rev.,* **116,** 2366–2387.

Takacs, L. L., A. Molod, and T. Wang, 1995: Documentation of the Goddard Earth Observing System (GEOS) General Circulation Model-Version 1. NASA Tech. Memo. 104606, Vol. 1, 100 pp. [Available from NASA Goddard Space Flight Center, Greenbelt, MD 20771, and online at http://dao.gsfc.nasa.gov/subpages/tech-reports.html.]

Thépaut, J.-N., P. Courtier, G. Belaud, and G. Lemaitre, 1996: Dynamical structure functions in a four-dimensional variational assimilation: A case study. *Quart. J. Roy. Meteor. Soc.,* **122,** 535–561.

Todling, R., S. E. Cohn, and N. S. Sivakumaran, 1998: Suboptimal schemes for retrospective data assimilation based on the fixed-lag Kalman smoother. *Mon. Wea. Rev.,* **126,** 2274–2286.